



Article

Structural and Electrochemical Characteristics of Platinum Nanoparticles Supported on Various Carbon Carriers

Margarita Kozlova ^{1,2}, Sergey Butrim ^{1,2}, Maksim Solovyev ^{1,2}, Artem Pushkarev ^{1,2}, Irina Pushkareva ^{1,2}, Valery Kalinichenko ^{2,3,4}, Svetlana Akelkina ² and Sergey Grigoriev ^{1,2,5,6,*}

- ¹ National Research University "Moscow Power Engineering Institute", 14, Krasnokazarmennaya St., 111250 Moscow, Russia; KozlovaMarV@mpei.ru (M.K.); ButrimSI@mpei.ru (S.B.); SolovyevMaxA@mpei.ru (M.S.); PushkarevAS@mpei.ru (A.P.); PushkarevaIV@mpei.ru (I.P.)
² National Research Centre, "Kurchatov Institute", 1, Akademika Kurchatova Sq., Moscow 123182, Russia; kalinval47@mail.ru (V.K.); akelkina_sv@nrcki.ru (S.A.)
³ N.M. Emanuel Institute of Biochemical Physics, Russian Academy of Sciences, 4, Kosygina St., 119991 Moscow, Russia
⁴ N.N. Semenov Federal Research Center for Chemical Physics, Russian Academy of Sciences, 4, Kosygina St., 119991 Moscow, Russia
⁵ HySA Infrastructure Center of Competence, Faculty of Engineering, North-West University, Potchefstroom 2531, South Africa
⁶ A.N. Nesmeyanov Institute of Organoelement Compounds, Russian Academy of Sciences, 28, Vavilova St., 119991 Moscow, Russia
* Correspondence: GrigoryevSA@mpei.ru; Tel.: +7-495-362-7206

Abstract: Graphene-like materials have attracted significant attention as alternative catalyst carriers due to the broad possibilities of changing their shape, composition, and properties. In this study we investigated the structural and electrochemical characteristics of platinum electrocatalysts supported on reduced graphene oxide (rGO), including those modified with amine functionalities, nitrogen heteroatoms (rGO-Am), and oxygen enriched (rGO-O). Synthesis of Pt nanoparticles (20 wt.%) on the graphene-like nanomaterials surface was carried out using a modified polyol procedure. The Pt²⁰/rGO-Am showed a lower Pt nanoparticles size together with high Pt utilization and EASA values compared to rGO-supported catalysts and the Pt/C reference sample due to the uniform distribution of nucleation centers on the surface of graphene nanoparticles, and the greater ability of these centers to electrically bond with platinum.

Keywords: reduced graphene oxide; aminated graphene; ozonized graphene; functionalized catalyst carrier; carbon-supported platinum nanoparticle; platinum utilization; functional group; polyol reduction; polymer electrolyte membrane fuel cell; PEMFC



Citation: Kozlova, M.; Butrim, S.; Solovyev, M.; Pushkarev, A.; Pushkareva, I.; Kalinichenko, V.; Akelkina, S.; Grigoriev, S. Structural and Electrochemical Characteristics of Platinum Nanoparticles Supported on Various Carbon Carriers. *C* **2022**, *8*, 14. <https://doi.org/10.3390/c8010014>

Academic Editor: Gil Goncalves

Received: 24 December 2021

Accepted: 4 February 2022

Published: 14 February 2022

Publisher's Note: MDPI stays neutral with regard to jurisdictional claims in published maps and institutional affiliations.



Copyright: © 2022 by the authors. Licensee MDPI, Basel, Switzerland. This article is an open access article distributed under the terms and conditions of the Creative Commons Attribution (CC BY) license (<https://creativecommons.org/licenses/by/4.0/>).

1. Introduction

Polymer electrolyte membrane fuel cells (PEMFC) are being developed as power sources for transport, stationary and portable systems as an alternative to conventional internal combustion engines, secondary batteries, and other conventional power sources [1]. The catalyst for the oxygen reduction reaction (ORR) (usually carbon-supported Pt nanoparticles [2]) is the main component of the membrane-electrode assembly (MEA) of PEMFC, which determines its performance, efficiency and durability [3]. The high specific surface area of catalysts based on Pt nanoparticles is achieved by using carbon carries [4]. Carbon carries must have such properties as: a high specific surface area, high electrical conductivity, developed pore structure and corrosion resistance [5]. In particular, in order to ensure the transport of reagents/reaction products to/from the active centers, the carbon supports must have a large number of mesopores and macropores, and an appropriate morphology [6]. The most commonly used carbon supports are carbon blacks (for example, Vulcan XC-72), which do not completely fulfil catalyst support requirements, especially on

the corrosion resistance [7,8]. The disadvantage of carbon black consists of its microporous structure. The metal particles may sink inside micropores, decreasing the electrochemically active surface area (EASA). This leads to the development of mesoporous carbons with high mesopores ($2 < \text{pore sizes} < 50 \text{ nm}$) degree. These materials have attracted a lot of attention due to their regular structure, high surface area, large pore volume and a narrow pore size distribution [9].

The challenging task is the development of alternative supports for Pt nanoparticles that increase the activity and stability of the catalyst, reduce the noble metal loading, and provide optimal properties of the active layer (hydrophobicity/hydrophilicity, porous structure, etc.) that allow the mass transfer facilitation [10,11]. Therefore, graphene-like materials and their derivatives are considered as promising catalyst supports.

Graphene first obtained by mechanical exfoliation [12] is significantly exploited for energy storage systems because of its excellent physical-chemical properties: high specific surface area (up to $2600 \text{ m}^2 \text{ g}^{-1}$), high thermal and electrical conductivity, corrosion resistance and mechanical strength (up to 130 GPa) [13]. In graphene, each carbon atom is covalently bonded with neighboring carbon atoms by three in-plane σ -bonds (from sp^2 orbitals) and one π -bond (from the remaining 2p orbital) perpendicular to the basal plane comprising the electron delocalization network [14,15]. For many electrochemical systems, including PEMFC, dispersed derivatives of graphene, such as three-dimensional reduced graphene oxide (rGO) are of practical interest [16,17]. Due to the sp^2 -hybridized carbon atoms the chemical and electrochemical stability of graphene-like materials are quite high [18,19], and these materials are considered as promising supports of Pt nanoparticles. However, the graphene basal plane is inert and does not have enough defects that could act as the active centers of electrochemical reactions or nucleation of nanoparticles [20]. Carbon materials modified with heteroatoms (B, N, S or P) allow for breaking the surface electroneutrality and redistributing the electronic density, providing the appearance of active centers for the deposition of Pt nanoparticles, as well as controlling their properties [21]. This allows for achieving higher activity and stability of electrocatalysts in ORR and other reactions compared with counterparts based on carbon black or graphene-like materials without doping [22]. In particular, aminated graphene exhibits complicated morphology with a tendency to form a wrinkled and corrugated structure, which facilitates the formation of porous films and aerogels, making it promising for catalyst and sensing applications [23].

The proposed study is focused on the structural, morphological and electrochemical properties of electrocatalysts supported on rGO modified with amine functionalities and nitrogen heteroatoms (rGO-Am), and an oxygen enriched one (rGO-O) obtained by ozone treatment. The synthesized catalysts (with 20 wt.% of Pt) were characterized using different techniques, including X-ray photoemission spectroscopy (XPS), X-ray diffraction (XRD), transmission electron microscopy (TEM), and cyclic voltammetry.

2. Materials and Methods

Graphene oxide (GO) was obtained by modified Hummers' method, as described in [24,25].

The rGO-O was obtained by ozone–oxygen mixture treatment which was performed at $20 \text{ }^\circ\text{C}$ by barrier discharge in the ozone generator "MEDOZONE" UOTA-60-01. The ozone concentration was $30\text{--}50 \text{ mg L}^{-1}$, and the processing was carried out for $40\text{--}50 \text{ min}$ until the ozone absorption stopped [26].

The rGO-Am was synthesized via the following three-stage approach. At the first stage, GO was treated with hydrobromic acid. At the second stage the brominated graphene oxide was subjected to ammonolysis with alcoholic ammonia solution. At the third stage the aminated graphene oxide was reduced with hydrazine.

Synthesis of rGO-supported Pt nanoparticles (20 wt.%) was carried out by a modified polyol reduction approach [27]. Briefly, $11.2 \text{ mL H}_2\text{PtCl}_6 \times 2\text{H}_2\text{O}$ was used as the platinum precursor, and 180 mL of ethylene glycol was used as the reducing agent. The synthesis

was carried out in a Drexel flask with argon flowing in the flask, which was kept at 75 °C for 2 h, and then heated to a reduction temperature of 180 °C, and kept for 1 h. Washing was performed by decantation six times. Pt supported on Vulcan XC-72 (Pt/C) was used as the reference catalyst (Prometheus R&D Ltd., Rostov-on-Don, Russia).

XRD (SmartLab SE X-ray Diffractometer, Rigaku SmartLab, Tokyo, Japan) was carried out using $\text{CuK}\alpha$ radiation. The diffraction data for Pt^{20}/C , $\text{Pt}^{20}/\text{rGO}$, $\text{Pt}^{20}/\text{rGO-O}$ and $\text{Pt}^{20}/\text{rGO-Am}$ catalyst were recorded for 2θ angles between 5° and 120°. The crystallite size of Pt nanoparticles (d) was determined by Debye–Scherrer’s equation:

$$d = \frac{K\lambda}{\beta \cos\theta} \quad (1)$$

where K is the Scherrer constant (for spherical particles with cubic symmetry is equal to 0.94), λ is the wavelength of the X-ray used (0.15406 nm), β is the full width of the diffraction peak at half maximum in radians (FWHM), and θ is the Bragg angle.

The morphological features of the catalysts were studied by transmission electron microscopy (TEM) using a TitanTM 80–300 S/TEM (“FEI”) (80–300 kV, space resolution by points is equal to 0.07–0.08 nm).

The XPS studies were performed using a PHOIBOS 150 (SPECS Surface Nano Analysis GmbH, Berlin, Germany) hemispherical analyzer and monochromatic Al $\text{K}\alpha$ radiation (Kurchatov Complex of Synchrotron and Neutron Investigation, NRC “Kurchatov Institute”, Moscow, Russia). Obtained spectrums (C 1s, O 1s, Pt 4f) were measured and processed according to the approach described in [28,29].

Electrochemical studies were performed using a potentiostat Solartron 1285 (AMETEK Inc., Berwyn, PA, USA) in a three-electrode cell using Ag/AgCl/sat. KCl solution reference electrode (Ag/AgCl), polished glassy carbon working electrode, and Pt wire counter electrode [27,28]. Cyclic voltammograms were measured using Ar-purged 0.5 M H_2SO_4 solution in the potential range of –0.15 to 1.2 V at the sweep rate of 20 mV s^{-1} .

Electrocatalytic ink consisting of 16 mg of catalyst and 8 mL of water was prepared by ultrasonic treatment using a probe ultrasonic homogenizer (Cole Parmer, Vernon Hills, IL, USA) for 20 s with the following treatment in an ultrasonic bath for 40 min. Then, a 10 μL inks aliquot was dropped onto the working electrode surface. The pretreatment of the working electrode was performed via cyclic voltammetry at 100 mV s^{-1} until the stable curve was obtained.

Electrochemical surface area was calculated from cyclic voltammetry analysis by using the following equation:

$$EASA = \left(\frac{Q}{Q_H * L_{Pt}} \right) * 10^{-1} \quad (2)$$

where Q is the charge associated with the adsorption/desorption of hydrogen monolayers (average value between anodic and cathodic sweep was taken) ($\mu\text{C cm}^{-2}$), L_{Pt} is the Pt loading on the working electrode (mg cm^{-2}), and Q_H is the charge required to oxidize the monolayer of hydrogen on a Pt surface ($\mu\text{C cm}^{-2}$) [30].

The total Pt surface area was calculated using the equation below, considering particles have spherical shape [28]:

$$S_{Pt} = \frac{6000}{p * d} \quad (3)$$

where S_{Pt} —the total surface area of Pt particles ($\text{m}^2 \text{g}^{-1}$), d —the Pt particle diameter (nm) taken as the mean value between d_{XRD} and d_{TEM} , p —the density of Pt (21.4 g m^{-3}).

The accessibility of the Pt nanoparticles and the catalytic layer connectivity could be analyzed using the Pt utilization. Pt utilization of 100% means that all Pt nanoparticles

are integrated into the entire electron conductivity network and are fully accessible by the electrolyte. The Pt utilization was calculated using the equation below:

$$U_{pt} = \left(\frac{EASA}{S_{pt}} \right) * 100 \quad (4)$$

where U_{pt} is the Pt utilization of the catalyst (%) [28,31].

3. Results and Discussion

TEM-micrographs of Pt²⁰/rGO, Pt²⁰/rGO-O and Pt²⁰/rGO-Am catalysts are shown on Figure 1. All catalysts exhibit a layered structure which is characterized by some extent of Pt nanoparticles agglomeration. Using well-known ImageJ software [32], an analysis of the size distribution of Pt nanoparticles were performed (no less than 100 particles for each catalyst have been taken into account). Pt nanoparticles are well-dispersed with a narrow size distribution in the range of 2–3 nm with an average size of 2.8, 2.5 and 2.4 nm for Pt²⁰/rGO, Pt²⁰/rGO-O and Pt²⁰/rGO-Am, respectively. However, rGO-supported Pt nanoparticles are characterized by agglomeration, which leads to a decrease in catalysts EASA [28,33]. Pt²⁰/rGO-Am has the smallest average nanoparticle size because the nitrogen doping of rGO allows for the formation of additional defects on the rGO basal surface, which provides additional active centers for stabilizing Pt nanoparticles during their deposition. This contributes to a more uniform distribution of smaller Pt nanoparticles [34,35]. It should be noted that the average sizes of Pt nanoparticles in all obtained rGO-based catalysts were lower compared to the commercial catalyst Pt²⁰/C (average size of 3.1 nm) which is taken as a well-known reference catalyst [36].

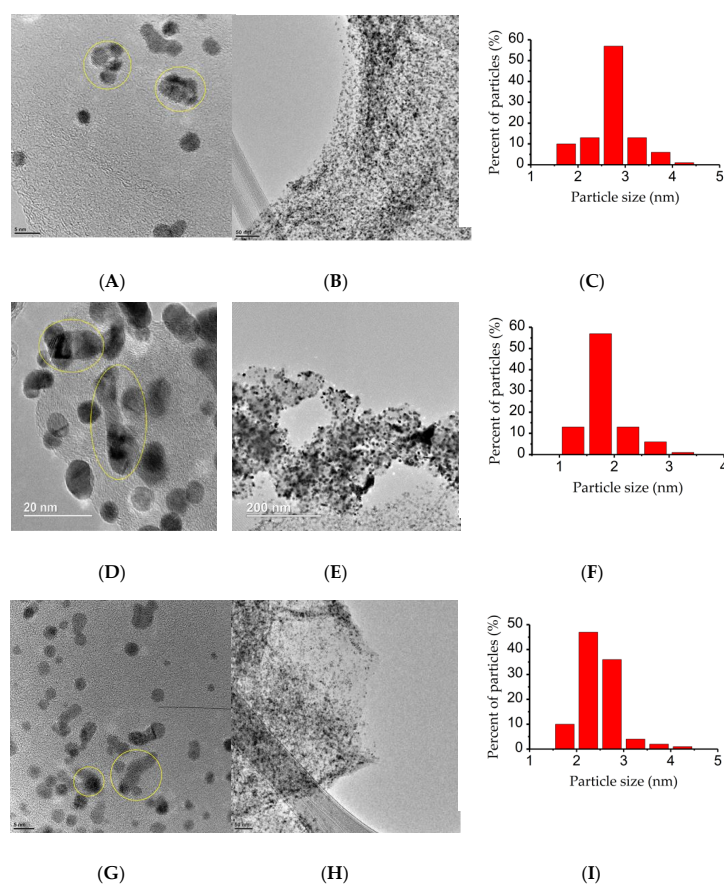


Figure 1. TEM images of Pt²⁰/rGO (A,B), Pt²⁰/rGO-O (D,E) and Pt²⁰/rGO-Am (G,H), the corresponding Pt nanoparticles size distribution (C,F,I).

In addition, the XRD investigations were performed to confirm the crystalline structures of the Pt on different supports (Figure 2). The characteristic peaks at $2\theta \approx 23.3^\circ$ with respect to the carbon (002) plane are detected for all studied catalysts. The diffraction peaks at 2θ of 39° , 46° , 67° , 81° and 85° correspond to the (111), (200), (220), (311) and (222) planes of the face-centered cubic structure of Pt crystallites, respectively [37]. The average crystallite size was calculated for the XRD peak assigned to Pt(220), as this is far from the background signal of carbon support [38]. The Pt crystallite size of Pt²⁰/C, Pt²⁰/rGO, Pt²⁰/rGO-O and Pt²⁰/rGO-Am was found to be ca. 2.83, 2.70, 2.85 and 2.69 nm, respectively. The obtained average crystallite sizes are given in Table 1 together with the particle sizes obtained by TEM. The mean Pt(220) crystallite size values are in a narrow range of 2.69–2.85 nm, which generally correlates well with the Pt nanoparticles mean size values (2.4–3.1 nm).

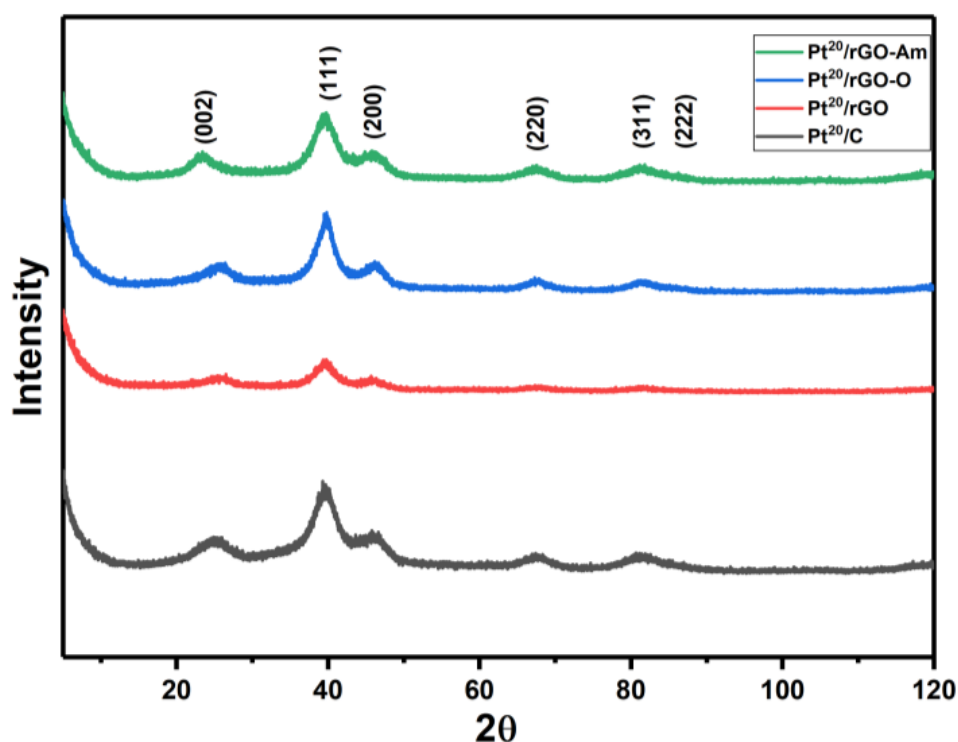


Figure 2. X-ray diffraction patterns for Pt²⁰/C, Pt²⁰/rGO, Pt²⁰/rGO-O and Pt²⁰/rGO-Am.

Table 1. Comparative parameters of the obtained catalysts.

Sample	d_{TEM} , nm	d_{XRD} , nm	EASA, $\text{m}^2 \text{g}^{-1}$	S_{Pt} , $\text{m}^2 \text{g}^{-1}$	U_{Pt} , %
Pt ²⁰ /C	3.1	2.83	70.5	94.7	77.4
Pt ²⁰ /rGO	2.8	2.70	67.1	101.9	65.8
Pt ²⁰ /rGO-O	2.5	2.85	40.6	105.0	25.8
Pt ²⁰ /rGO-Am	2.4	2.69	87.5	110.3	79.3

The elemental composition of Pt²⁰/rGO, Pt²⁰/rGO-O and Pt²⁰/rGO-Am catalysts was studied using X-ray photoelectron spectroscopy. According to the C 1s spectra (Figure 3A,C,E), rGO-supported catalysts primarily consist of sp²-carbon (~284.4 eV). The sp²/sp³ ratios of Pt²⁰/rGO, Pt²⁰/rGO-O and Pt²⁰/rGO-Am are 38.69, 23.4 and 1.23.

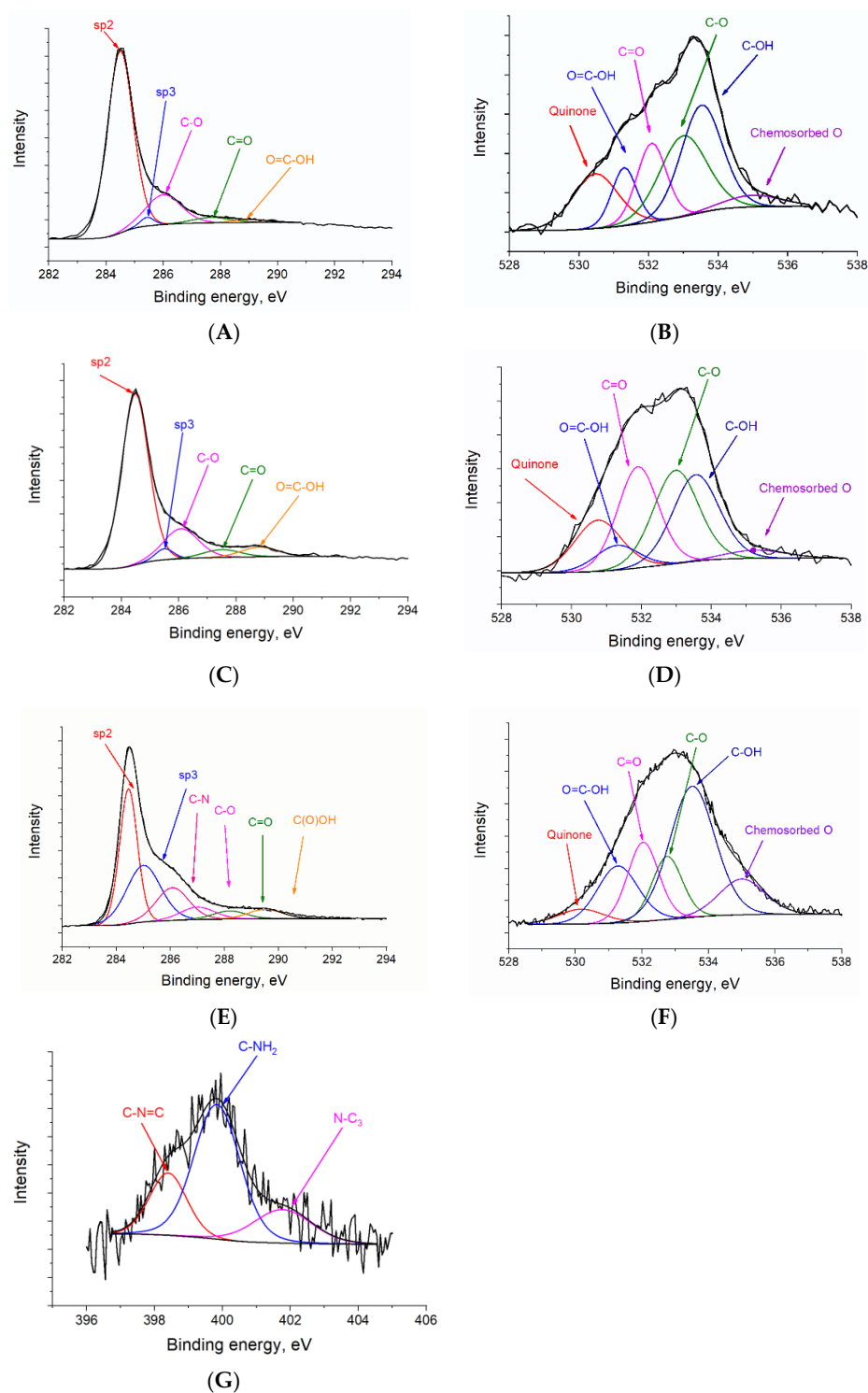


Figure 3. C 1s (A,C,E), O 1s (B,D,F) and N 1s (G) spectrums of catalysts: Pt²⁰/rGO (A,B), Pt²⁰/rGO-O (C,D) and Pt²⁰/rGO-Am (E,F,G).

According to the C 1s spectra, Pt²⁰/rGO and Pt²⁰/rGO-O are rather similar to each other and differ mainly in the relative intensity ratios of O=C-OH, C=O, C-O, C-OH and quinone groups [29]. The existence of C-N bonds (286.07 eV) [39], as well as relatively high sp³ carbon atoms ratios, should be noticed in Pt²⁰/rGO-Am.

The O 1s spectra of catalysts are characterized by several peaks and allow for a somewhat more detailed assessment of the oxygen-containing groups. In particular, quinone (~530.3–530.5 eV), carboxyl (~531.1 eV), carbonyl (~532.1 eV), C-O (~532.7–533.0 eV), and

hydroxyl (~533.7 eV) functional groups [29,40] are detected. Lower binding energy peaks in the O 1s spectra could be ascribed to the quinone [41] or Me-O. The existence of oxygen functional groups in rGO is due to the incomplete thermal reduction of graphene oxide at temperatures below 2000 °C [42]. The C/O value of each catalyst shows oxygen content and equals to 15.57, 9.35 and 8.87 at.% for Pt²⁰/rGO, Pt²⁰/rGO-O and Pt²⁰/rGO-Am, respectively. As such, the ozone treatment allows for significantly increasing the concentration of oxygen functional groups in comparison with the bare rGO, which is in good agreement with the literature. Ozone treatment of carbon black at 140 °C was responsible for a C/O decrease from 22.4 to 18.4 and increase in the oxygen functionalities content, especially in the carboxyl groups [43].

It is worth noting that the N 1s peak in Pt²⁰/rGO-Am confirms the presence of N in the rGO structure, according to XPS spectrum fitting the nitrogen content in rGO is ca. 1.41 at.% (Table 2). Thus, the peaks observed in Pt²⁰/rGO-Am spectra (Figure 3G) show the presence of amino groups (399.83 eV) [23], and demonstrate that the significant part of the N atoms being embedded in the rGO structure in the form of quaternary N (401.78 eV) and pyridine N (398.4 eV) [29,44]. It is important to note that the amine functionality with its peak area percentage of ca. 60% appears to be a dominant type of nitrogen species. The dominance of amine functionality was reported for bare aminated rGO as well [23]. It is well known that amino, carbonyl and carboxyl groups can replace chlorine in the coordination sphere of hexachloroplatinates [45–47]. The introduction of functional groups into the rGO allows for the immobilization of platinum precursor molecules (H₂PtCl₆) on the support surface. The features of these groups determine the Pt nanoparticles morphology. Moreover, the nitrogen heteroatoms presumably contribute to better Pt nanoparticles distribution, as described recently [48–50].

Table 2. Some results of XPS spectrums fitting of Pt²⁰/rGO, Pt²⁰/rGO-O and Pt²⁰/rGO-Am.

Sample	C/O	C sp ² , %	N, at.%	NH ₂ -, %	N _{pyr} , %	N _{quat} , %
Pt ²⁰ /rGO	15.57	76.2	–	–	–	–
Pt ²⁰ /rGO-O	9.35	71.1	–	–	–	–
Pt ²⁰ /rGO-Am	8.87	37.0	1.41	59.57	21.98	18.43

Metallic Pt (0) duplet peaks were detected at 71.20/74.55 eV, 71.22/74.57 eV and 71.39/74.72 eV for Pt²⁰/rGO, Pt²⁰/rGO-O and Pt²⁰/rGO-Am (Figure 4). The Pt (0) content of Pt²⁰/rGO, Pt²⁰/rGO-O and Pt²⁰/rGO-Am is ca. 46.18, 52.77 and 55.4%, respectively. The observed binding energy shift (ca. 0.2 eV) of the Pt/rGO-Am catalyst Pt(0) peak toward higher values is associated with a change in the electronic structure of the support (downshifting of the *d*-band center position), which may decrease the specific interaction between the Pt surface and strongly adsorbed intermediates (e.g., OH_{ads}) [51]. Moreover, the decrease in these adsorbed OH_{ads}-Pt interactions could enhance the catalytic activity of Pt towards ORR [52,53]. This is consistent with the apparent absence of Pt (IV) in the Pt 4f spectrum (Figure 4C) [54].

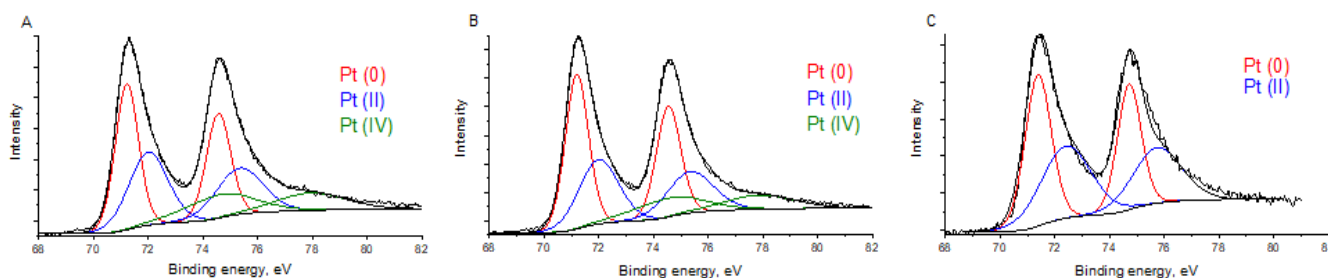


Figure 4. Spectra Pt 4f of Pt²⁰/rGO (A), Pt²⁰/rGO-O (B) and Pt²⁰/rGO-Am (C) catalysts obtained by the XPS method.

The cyclic voltammograms of catalysts of Pt²⁰/C, Pt²⁰/rGO, Pt²⁰/rGO-O, Pt²⁰/rGO-Am are shown in Figure 5. Well-defined peaks, observed in the potential range from −0.15 to 0.2 V vs. Ag/AgCl reference electrode correspond to the desorption/adsorption of the hydrogen monolayer on the surface of Pt nanoparticles [28]. The EASA value for Pt²⁰/C, Pt²⁰/rGO, Pt²⁰/rGO-O and Pt²⁰/rGO-Am is ca. 70.5, 67.1, 40.6 and 87.5 m² g^{−1}, respectively. The EASA value for Pt²⁰/rGO is in good agreement with the data reported in the literature [55] for the rGO-supported catalyst (52.1 m² g^{−1}) with a similar platinum content and rather close mean Pt nanoparticle size. Pt²⁰/rGO-O has low EASA, presumably due to a high degree of particle agglomeration during synthesis. These areas are unevenly distributed over the rGO surface, and tend to appear near the graphene sheet edges. Therefore, Pt nanoparticles in Pt²⁰/rGO-O tend to be closely formed on the same areas, allowing their aggregation [26]. This could be responsible for lower catalyst EASA and Pt utilization, as discussed below.

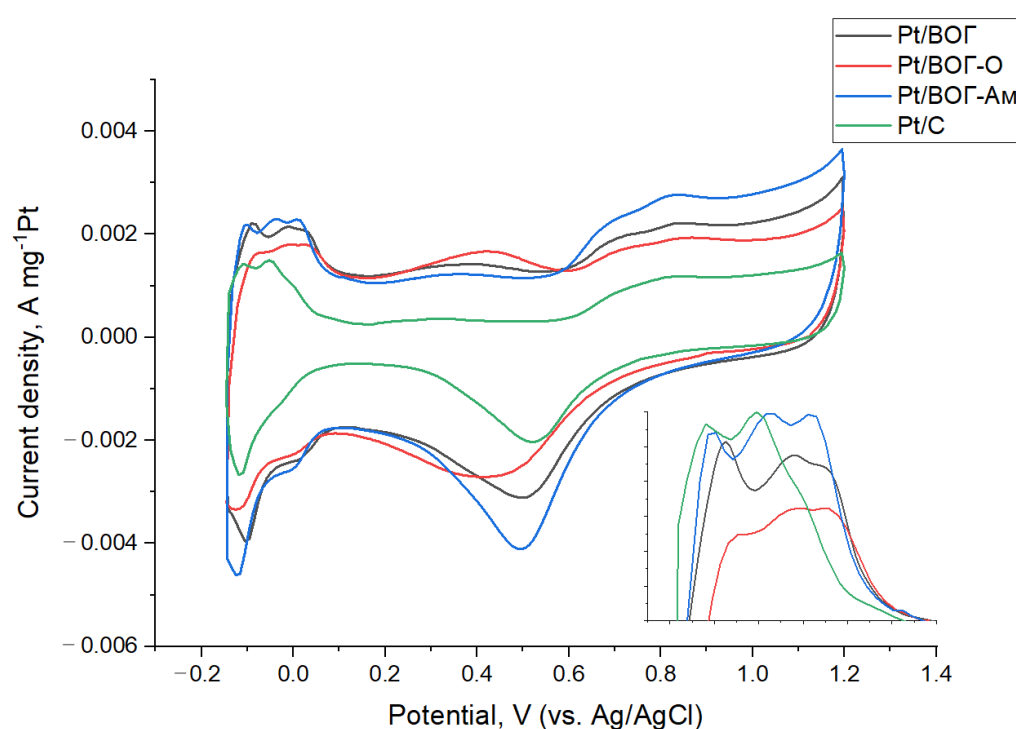


Figure 5. Cyclic voltammograms of Pt²⁰/C, Pt²⁰/rGO, Pt²⁰/rGO-O and Pt²⁰/rGO-Am measured in an Ar-purged 0.5 M H₂SO₄ solution at 20 mV s^{−1}.

The purpose of studying the Pt utilization in the electrocatalyst is to evaluate the electronic bonding of the carbon support with Pt nanoparticles [56]. According to our results, the obtained EASA values are lower than the values of the total Pt surface area calculated from Equation (3), even using a low-loaded thin catalytic film on the working electrode surface. Pt utilization of the various rGO-supported catalyst could vary from 28% to 93% [57,58] depending on synthesis approach and conditions. The obtained results (Table 1) show that the nitrogen doping of rGO allows for increasing the catalyst EASA, reducing the Pt nanoparticles agglomeration degree, and increasing the Pt utilization. This observation is in good agreement with the literature; the interaction between Pt nanoparticles and the N-doped support enhance adhesion of the Pt nanoparticles to the support [35] which could alleviate the aggregation of the nanoparticles. Moreover, first-principles study revealed that Pt nucleation is favorable on pyridinic and pyrrolic N, and the center of the *d*-band can be shifted downward by the nitrogen species [52]. The EASA of Pt²⁰/rGO and Pt²⁰/rGO-O catalysts calculated by CVs exhibited low values compared to Pt²⁰/C, which is probably due to the blocking on the surface of the Pt particles and to the inaccessibility of the catalyst deep inside the micropores of the carbon support [59].

4. Conclusions

In this study, variously modified rGO-based catalytic materials were synthesized and characterized, and their performances were compared with those for a reference Pt/C catalyst. The aminated rGO synthesized in this study could be suggested as a promising PEMFC catalyst support due to the uniform distribution of Pt nanoparticles provided by amino functionalities and embedded nitrogen (pyridine and quaternary) heteroatoms. Amination provides additional sites for Pt nanoparticles nucleation and prevents their further growth during synthesis. The low nanoparticles agglomeration degree ensures a high Pt utilization value, which is higher than the one for the bare rGO-supported catalyst and comparable with those for Pt/C. Pt²⁰/rGO-Am catalyst showed the highest % ECSA among the other catalysts. Ozone treatment of rGO is still a questionable approach, as the Pt nanoparticles morphology is not appropriate for further use as PEMFC catalyst, because of the high degree of catalyst particles agglomeration, which deteriorates the catalyst layer microstructure, thus reducing the MEA performance.

Author Contributions: Conceptualization, M.K., A.P. and I.P.; methodology, I.P., S.B. and M.S.; validation, M.K., A.P. and S.A.; investigation, M.K. and V.K.; resources, S.G.; writing—original draft preparation, M.K. and A.P.; writing—review and editing, I.P. and S.G.; visualization, M.K. and I.P.; supervision, S.G.; project administration, S.G. and I.P.; funding acquisition, S.G. and A.P. All authors have read and agreed to the published version of the manuscript.

Funding: This work has been performed within the framework of the project “Modified carbon nanomaterials for electrodes of fuel cells with solid polymer electrolyte”, with the support of a grant from the National Research University “Moscow Power Engineering Institute” for the implementation of scientific research programs “Energy”, “Electronics, Radio Engineering and IT”, and “Industry 4.0 Technologies for Industry and Robotics in 2020–2022”.

Institutional Review Board Statement: Not applicable.

Informed Consent Statement: Not applicable.

Acknowledgments: Thanks to E.V. Kukueva for capturing the TEM images, to R.G. Chumakov for capturing and processing of the XPS spectrums, and to V.V. Podmasterijev for RGO ozone processing.

Conflicts of Interest: The authors declare no conflict of interest. The funders had no role in the design of the study; in the collection, analyses, or interpretation of data; in the writing of the manuscript, or in the decision to publish the results.

References

1. Abdelkareem, M.A.; Elsaid, K.; Wilberforce, T.; Kamil, M.; Sayed, E.T.; Olabi, A. Environmental aspects of fuel cells: A review. *Sci. Total Environ.* **2021**, *752*, 141803. [[CrossRef](#)] [[PubMed](#)]
2. Wang, Y.; Ruiz Diaz, D.F.; Chen, K.S.; Wang, Z.; Adroher, X.C. Materials, technological status, and fundamentals of PEM fuel cells—A review. *Mater. Today* **2020**, *32*, 178–203. [[CrossRef](#)]
3. Hou, J.; Yang, M.; Ke, C.; Wei, G.; Priest, C.; Qiao, Z.; Wu, G.; Zhang, J. Platinum-group-metal catalysts for proton exchange membrane fuel cells: From catalyst design to electrode structure optimization. *EnergyChem* **2020**, *2*, 100023. [[CrossRef](#)]
4. Du, L.; Shao, Y.; Sun, J.; Yin, G.; Liu, J.; Wang, Y. Advanced catalyst supports for PEM fuel cell cathodes. *Nano Energy* **2016**, *29*, 314–322. [[CrossRef](#)]
5. Lee, J.-H.; Park, S.-J. Recent advances in preparations and applications of carbon aerogels: A review. *Carbon* **2020**, *163*, 1–18. [[CrossRef](#)]
6. Grigoriev, S.A.; Millet, P.; Fateev, V.N. Evaluation of carbon-supported Pt and Pd nanoparticles for the hydrogen evolution reaction in PEM water electrolyzers. *J. Power Source* **2008**, *177*, 281–285. [[CrossRef](#)]
7. Zhang, S.; Yuan, X.-Z.; Hin, J.N.C.; Wang, H.; Friedrich, K.A.; Schulze, M. A review of platinum-based catalyst layer degradation in proton exchange membrane fuel cells. *J. Power Source* **2009**, *194*, 588–600. [[CrossRef](#)]
8. Bharti, A.; Cheruvally, G. Influence of various carbon nano-forms as supports for Pt catalyst on proton exchange membrane fuel cell performance. *J. Power Source* **2017**, *360*, 196–205. [[CrossRef](#)]
9. Messias, S.; Nunes da Ponte, M.S.; Reis-Machado, A. Carbon Materials as Cathode Constituents for Electrochemical CO₂ Reduction—A Review. *C—J. Carbon Res.* **2019**, *5*, 83. [[CrossRef](#)]
10. Pak Hoe, L.; Boaventura, M.; Lagarteira, T.; Kee Shyuan, L.; Mendes, A. Polyol synthesis of reduced graphene oxide supported platinum electrocatalysts for fuel cells: Effect of Pt precursor, support oxidation level and pH. *Int. J. Hydrogen Energy* **2018**, *43*, 16998–17011. [[CrossRef](#)]

11. Baranov, I.E.; Grigoriev, S.A.; Ylitalo, D.; Fateev, V.N.; Nikolaev, I.I. Transfer processes in PEM fuel cell: Influence of electrode structure. *Int. J. Hydrogen Energy* **2006**, *31*, 203–210. [[CrossRef](#)]
12. Geim, A.K.; Novoselov, K.S. The rise of graphene. *Nanosci. Technol.* **2009**, *6*, 11–19.
13. Jamil, M.F.; Biçer, E.; Yazar Kaplan, B.; Alkan Gürsel, S. One-step fabrication of new generation graphene-based electrodes for polymer electrolyte membrane fuel cells by a novel electrophoretic deposition. *Int. J. Hydrogen Energy* **2021**, *46*, 5653–5663. [[CrossRef](#)]
14. Bera, M.; Maji, P.K. Effect of structural disparity of graphene-based materials on thermo-mechanical and surface properties of thermoplastic polyurethane nanocomposites. *Polymer* **2017**, *119*, 118–133. [[CrossRef](#)]
15. Armano, A.; Agnello, S. Two-Dimensional Carbon: A Review of Synthesis Methods, and Electronic, Optical, and Vibrational Properties of Single-Layer Graphene. *C—J. Carbon Res.* **2019**, *5*, 67. [[CrossRef](#)]
16. Alekseeva, O.K.; Pushkareva, I.V.; Pushkarev, A.S.; Fateev, V.N. Graphene and Graphene-Like Materials for Hydrogen Energy. *Nanotechnol. Russ.* **2020**, *15*, 273–300. [[CrossRef](#)]
17. Tkachev, S.V.; Buslaeva, E.Y.; Naumkin, A.V.; Kotova, S.L.; Laure, I.V.; Gubin, S.P. Reduced graphene oxide. *Inorg. Mater.* **2012**, *48*, 796–802. [[CrossRef](#)]
18. Erickson, K.; Erni, R.; Lee, Z.; Alem, N.; Gannett, W.; Zettl, A. Determination of the Local Chemical Structure of Graphene Oxide and Reduced Graphene Oxide. *Adv. Mater.* **2010**, *22*, 4467–4472. [[CrossRef](#)]
19. Mamat, M.; Grigoriev, S.; Dzhus, K.; Grant, D.; Walker, G. The performance and degradation of Pt electrocatalysts on novel carbon carriers for PEMFC applications. *Int. J. Hydrogen Energy* **2010**, *35*, 7580–7587. [[CrossRef](#)]
20. Su, H.; Hu, Y.H. Recent advances in graphene-based materials for fuel cell applications. *Energy Sci. Eng.* **2021**, *9*, 958–983. [[CrossRef](#)]
21. Feng, X.; Bai, Y.; Liu, M.; Li, Y.; Yang, H.; Wang, X.; Wu, C. Untangling the respective effects of heteroatom-doped carbon materials in batteries, supercapacitors and the ORR to design high performance materials. *Energy Environ. Sci.* **2021**, *14*, 2036–2089. [[CrossRef](#)]
22. Shahgaldi, S.; Hamelin, J. Improved carbon nanostructures as a novel catalyst support in the cathode side of PEMFC: A critical review. *Carbon* **2015**, *94*, 705–728. [[CrossRef](#)]
23. Rabchinskii, M.K.; Ryzhkov, S.A.; Kirilenko, D.A.; Ulin, N.V.; Baidakova, M.V.; Shnitov, V.V.; Pavlov, S.I.; Chumakov, R.G.; Stolyarova, D.Y.; Besedina, N.A.; et al. From graphene oxide towards aminated graphene: Facile synthesis, its structure and electronic properties. *Sci. Rep.* **2020**, *10*, 6902. [[CrossRef](#)] [[PubMed](#)]
24. Pushkarev, A.S.; Pushkareva, I.V.; Grigoriev, S.A.; Kalinichenko, V.N.; Presniakov, M.Y.; Fateev, V.N. Electrocatalytic layers modified by reduced graphene oxide for PEM fuel cells. *Int. J. Hydrogen Energy* **2015**, *40*, 14492–14497. [[CrossRef](#)]
25. Grigor'ev, S.A.; Pushkarev, A.S.; Kalinichenko, V.N.; Pushkareva, I.V.; Presnyakov, M.Y.; Fateev, V.N. Electrocatalytic layers based on reduced graphene oxide for fabrication of low-temperature fuel cells. *Kinet. Catal.* **2015**, *56*, 689–693. [[CrossRef](#)]
26. Grigoriev, S.A.; Fateev, V.N.; Pushkarev, A.S.; Pushkareva, I.V.; Ivanova, N.A.; Kalinichenko, V.N.; Presnyakov, M.Y.; Wei, X. Reduced Graphene Oxide and Its Modifications as Catalyst Supports and Catalyst Layer Modifiers for PEMFC. *Materials* **2018**, *11*, 1405. [[CrossRef](#)]
27. Pushkarev, A.S.; Pushkareva, I.V.; Ivanova, N.A.; du Preez, S.; Bessarabov, D.G.; Chumakov, R.G.; Stankevich, V.G.; Fateev, V.N.; Evdokimov, A.A.; Grigoriev, S.A. Pt/C and Pt/SnO_x/C Catalysts for Ethanol Electrooxidation: Rotating Disk Electrode Study. *Catalysts* **2019**, *9*, 271. [[CrossRef](#)]
28. Pushkareva, I.V.; Pushkarev, A.S.; Kalinichenko, V.N.; Chumakov, R.G.; Soloviev, M.A.; Liang, Y.; Millet, P.; Grigoriev, S.A. Reduced Graphene Oxide-Supported Pt-Based Catalysts for PEM Fuel Cells with Enhanced Activity and Stability. *Catalysts* **2021**, *11*, 256. [[CrossRef](#)]
29. Pushkarev, A.S.; Alekseeva, O.K.; Pushkareva, I.V.; Shapir, B.L.; Chumakov, R.G.; Tishkin, V.V.; Kozlova, M.V.; Kalinichenko, V.N.; Fateev, V.N. Plasma doping of nanostructured reduced graphene oxide. *Nanotechnol. Russ.* **2020**, *15*, 735–740. [[CrossRef](#)]
30. Pozio, A.; Francesco, M.; De Cemmi, A.; Cardellini, F.; Giorgi, L.; De Francesco, M.; Cemmi, A.; Cardellini, F.; Giorgi, L. Comparison of high surface Pt/C catalysts by cyclic voltammetry. *J. Power Source* **2002**, *105*, 13–19. [[CrossRef](#)]
31. Avcioglu, G.S.; Ficilar, B.; Bayrakceken, A.; Eroglu, I. High performance PEM fuel cell catalyst layers with hydrophobic channels. *Int. J. Hydrogen Energy* **2015**, *40*, 7720–7731. [[CrossRef](#)]
32. Schneider, C.A.; Rasband, W.S.; Eliceiri, K.W. NIH Image to ImageJ: 25 years of image analysis. *Nat. Methods* **2012**, *9*, 671–675. [[CrossRef](#)] [[PubMed](#)]
33. Spasov, D.D.; Ivanova, N.A.; Pushkarev, A.S.; Pushkareva, I.V.; Presnyakova, N.N.; Chumakov, R.G.; Presnyakov, M.Y.; Grigoriev, S.A.; Fateev, V.N. On the Influence of Composition and Structure of Carbon-Supported Pt-SnO₂ Hetero-Clusters onto Their Electrocatalytic Activity and Durability in PEMFC. *Catalysts* **2019**, *9*, 803. [[CrossRef](#)]
34. Puthusseri, D.; Ramaprabhu, S. Oxygen reduction reaction activity of platinum nanoparticles decorated nitrogen doped carbon in proton exchange membrane fuel cell under real operating conditions. *Int. J. Hydrogen Energy* **2016**, *41*, 13163–13170. [[CrossRef](#)]
35. Melke, J.; Peter, B.; Habereeder, A.; Ziegler, J.; Fasel, C.; Nefedov, A.; Sezen, H.; Wöll, C.; Ehrenberg, H.; Roth, C. Metal-Support Interactions of Platinum Nanoparticles Decorated N-Doped Carbon Nanofibers for the Oxygen Reduction Reaction. *ACS Appl. Mater. Interfaces* **2016**, *8*, 82–90. [[CrossRef](#)]
36. Nefedkin, S.I.; Guterman, V.E.; Alekseenko, A.A.; Belenov, S.V.; Ivanenko, A.V.; Klimova, M.A.; Pavlov, V.I.; Panov, S.V.; Paperzh, K.O.; Shubenkov, S.V. Russian Technologies and Nanostructural Materials in High Specific Power Systems Based on Hydrogen–Air Fuel Cells with an Open Cathode. *Nanotechnol. Russ.* **2020**, *15*, 370–378. [[CrossRef](#)]

37. Carrera-Cerritos, R.; Baglio, V.; Aricò, A.S.; Ledesma-García, J.; Sgroi, M.F.; Pullini, D.; Pruna, A.J.; Mataix, D.B.; Fuentes-Ramírez, R.; Arriaga, L.G. Improved Pd electro-catalysis for oxygen reduction reaction in direct methanol fuel cell by reduced graphene oxide. *Appl. Catal. B Environ.* **2014**, *144*, 554–560. [[CrossRef](#)]
38. Hyun, K.; Lee, J.H.; Yoon, C.W.; Kwon, Y. The Effect of Platinum Based Bimetallic Electrocatalysts on Oxygen Reduction Reaction of Proton Exchange Membrane Fuel Cells. *Int. J. Electrochem. Sci.* **2013**, *8*, 11752–11767.
39. Ma, J.; Habrioux, A.; Luo, Y.; Ramos-Sanchez, G.; Calvillo, L.; Granozzi, G.; Balbuena, P.B.; Alonso-Vante, N. Electronic interaction between platinum nanoparticles and nitrogen-doped reduced graphene oxide: Effect on the oxygen reduction reaction. *J. Mater. Chem. A* **2015**, *3*, 11891–11904. [[CrossRef](#)]
40. Stobinski, L.; Lesiak, B.; Malolepszy, A.; Mazurkiewicz, M.; Mierzwa, B.; Zemek, J.; Jiricek, P.; Bieloshapka, I. Graphene oxide and reduced graphene oxide studied by the XRD, TEM and electron spectroscopy methods. *J. Electron Spectros. Relat. Phenom.* **2014**, *195*, 145–154. [[CrossRef](#)]
41. Oh, Y.J.; Yoo, J.; Kim, Y.I.; Yoon, J.K.; Na Yoon, H.; Kim, J.-H.; Bin Park, S. Oxygen functional groups and electrochemical capacitive behavior of incompletely reduced graphene oxides as a thin-film electrode of supercapacitor. *Electrochim. Acta* **2014**, *116*, 118–128. [[CrossRef](#)]
42. Botas, C.; Álvarez, P.; Blanco, C.; Santamaría, R.; Granda, M.; Gutiérrez, M.D.; Rodríguez-Reinoso, F.; Menéndez, R. Critical temperatures in the synthesis of graphene-like materials by thermal exfoliation–reduction of graphite oxide. *Carbon* **2013**, *52*, 476–485. [[CrossRef](#)]
43. Chang, X.; Dong, F.; Yang, S.; Tang, Z.; Zha, F. Well dispersed Pt nanoparticles on commercial carbon black oxidized by ozone possess significantly high electro-catalytic activity for methanol oxidation. *Int. J. Hydrogen Energy* **2019**, *44*, 21559–21568. [[CrossRef](#)]
44. Deng, Y.; Xie, Y.; Zou, K.; Ji, X. Review on recent advances in nitrogen-doped carbons: Preparations and applications in supercapacitors. *J. Mater. Chem. A* **2016**, *4*, 1144–1173. [[CrossRef](#)]
45. Zou, M.; Du, M.; Zhang, M.; Yang, T.; Zhu, H.; Wang, P.; Bao, S. Synthesis and deposition of ultrafine noble metallic nanoparticles on amino-functionalized halloysite nanotubes and their catalytic application. *Mater. Res. Bull.* **2015**, *61*, 375–382. [[CrossRef](#)]
46. Golovizin, V.S.; Levchenko, L.M. Recovery of Platinum Complexes from Chloride Solutions Using Oxidized Carbon Sorbents. *Chem. Sustain. Dev.* **2011**, *19*, 537–540.
47. Kim, K.T.; Kim, Y.G.; Chung, J.S. Adsorption of cationic platinum complex onto carbon support. *Carbon* **1993**, *31*, 1289–1296.
48. Li, Z.; Gao, Q.; Zhang, H.; Tian, W.; Tan, Y.; Qian, W.; Liu, Z. Low content Pt nanoparticles anchored on N-doped reduced graphene oxide with high and stable electrocatalytic activity for oxygen reduction reaction. *Sci. Rep.* **2017**, *7*, 43352. [[CrossRef](#)]
49. Mao, S.; Wang, C.; Wang, Y. The chemical nature of N doping on N doped carbon supported noble metal catalysts. *J. Catal.* **2019**, *375*, 456–465. [[CrossRef](#)]
50. Zhao, L.; Sui, X.-L.; Li, J.-L.; Zhang, J.-J.; Zhang, L.-M.; Wang, Z.-B. Ultra-fine Pt nanoparticles supported on 3D porous N-doped graphene aerogel as a promising electro-catalyst for methanol electrooxidation. *Catal. Commun.* **2016**, *86*, 46–50.
51. Zhu, J.; Xiao, M.; Zhao, X.; Liu, C.; Ge, J.; Xing, W. Strongly coupled Pt nanotubes/N-doped graphene as highly active and durable electrocatalysts for oxygen reduction reaction. *Nano Energy* **2015**, *13*, 318–326. [[CrossRef](#)]
52. Tachibana, N.; Yukawa, Y.; Morikawa, K.; Kawaguchi, M.; Shimanoe, K. Pt nanoparticles supported on nitrogen-doped porous carbon as efficient oxygen reduction catalysts synthesized via a simple alcohol reduction method. *SN Appl. Sci.* **2021**, *3*, 338. [[CrossRef](#)]
53. Nie, Y.; Wei, Z. Surface-confined Pt-based catalysts for strengthening oxygen reduction performance. *Prog. Nat. Sci. Mater. Int.* **2020**, *30*, 796–806. [[CrossRef](#)]
54. Yazar Kaplan, B.; Haghmoradi, N.; Biçer, E.; Merino, C.; Alkan Gürsel, S. High performance electrocatalysts supported on graphene based hybrids for polymer electrolyte membrane fuel cells. *Int. J. Hydrogen Energy* **2018**, *43*, 23221–23230. [[CrossRef](#)]
55. Antony, R.P.; Preethi, L.K.; Gupta, B.; Mathews, T.; Dash, S.; Tyagi, A.K. Efficient electrocatalytic performance of thermally exfoliated reduced graphene oxide-Pt hybrid. *Mater. Res. Bull.* **2015**, *70*, 60–67. [[CrossRef](#)]
56. Avcioglu, G.S.; Ficicilar, B.; Eroglu, I. Improved PEM fuel cell performance with hydrophobic catalyst layers. *Int. J. Hydrogen Energy* **2018**, *43*, 18632–18641. [[CrossRef](#)]
57. Eris, S.; Daşdelen, Z.; Yıldız, Y.; Sen, F. Nanostructured Polyaniline-rGO decorated platinum catalyst with enhanced activity and durability for Methanol oxidation. *Int. J. Hydrogen Energy* **2018**, *43*, 1337–1343. [[CrossRef](#)]
58. Şanlı, L.I.; Bayram, V.; Yazar, B.; Ghobadi, S.; Gürsel, S.A. Development of graphene supported platinum nanoparticles for polymer electrolyte membrane fuel cells: Effect of support type and impregnation–reduction methods. *Int. J. Hydrogen Energy* **2016**, *41*, 3414–3427. [[CrossRef](#)]
59. Joo, S.H.; Pak, C.; You, D.J.; Lee, S.-A.; Lee, H.I.; Kim, J.M.; Chang, H.; Seung, D. Ordered mesoporous carbons (OMC) as supports of electrocatalysts for direct methanol fuel cells (DMFC): Effect of carbon precursors of OMC on DMFC performances. *Electrochim. Acta* **2006**, *52*, 1618–1626. [[CrossRef](#)]